Available online at www.sciencedirect.com

SciVerse ScienceDirect

Ceramics International 39 (2013) 3359–3364

CERAMICS INTERNATIONAL

www.elsevier.com/locate/ceramint

Short communication

# Nano-sized spinel $LiMn_2O_4$ powder fabricated *via* modified dynamic hydrothermal synthesis

Jinhan Yao[a,*], Longteng Lv[a], Chaoqi Shen[a], Pinjie Zhang[a], Kondo-Francois Aguey-Zinsou[b], Lianbang Wang[a,*]

[a]*State Key Laboratory Breeding Base of Green Chemistry-Synthesis Technology, College of Chemical Engineering and Material Science, Zhejiang University of Technology, Hangzhou, Zhejiang, PR China*

[b]*School of Chemical Engineering, The University of New South Wales, Sydney, Australia*

Received 25 July 2012; received in revised form 28 July 2012; accepted 28 July 2012
Available online 5 August 2012

**Abstract**

Nano-sized spinel $LiMn_2O_4$ powder with high crystallinity was prepared by a modified dynamic hydrothermal route. The as-synthesized $LiMn_2O_4$ powder exhibited high phase purity and better electrochemical properties than the material obtained *via* the static hydrothermal synthetic route. The dynamic method is believed to promote the simultaneous nucleation and growth of the $LiMn_2O_4$ phase during the synthesis.


*Keywords:* Spinel $LiMn_2O_4$; Dynamic hydrothermal synthesis; Nano-particles

## 1. Introduction

The selection of synthesis route is crucial to promote the application of spinel $LiMn_2O_4$ in high power Li-ion batteries. Spinel $LiMn_2O_4$ has attracted special interest for high power Li-ion batteries because of its significant advantages in terms of environmental acceptability, high safety, low price and high potential [1–5]. Electrochemical performance of $LiMn_2O_4$ is closely correlated to the material synthesis and thus the synthetic route and associated parameters would strongly influence the final properties of $LiMn_2O_4$. Commercialized $LiMn_2O_4$ spinel are prepared through the solid-state reaction of oxides and carbonates at temperatures as high as 700–900 °C [6–8]. The final product generally contains various irregular particles with a broad size distribution, as well as impurity phases. Besides, it is difficult to control the crystalline growth, compositional homogeneity and surface morphology. Soft chemical routes, such as Pechini, sol–gel, emulsion, melt-impregnation and spray-drying have been proposed [3–9], however so far all these methods suffer from high temperature heat treatment leading to an excessive coarsening of grain and particle sizes, the use of expensive reagents, and remain based on complex synthetic processes difficult to implement at large scales.

An alternative synthetic route rests upon the use of hydrothermal methods [10–13]. However, conventional static hydrothermal processes usually require longer reaction times (up to several days) because of the lack of frequent contact between the reactants remaining as precipitates at the bottom of hydrothermal reactor [12,13]. As a result, additional oxidants and reductants such as $H_2O_2$ and glucose have to be used together with the manganese source in order to improve the overall reaction kinetic [10,11]. This obviously leads to more complexity in the synthetic process as an increase in the number of reactants would lead to side reactions and thus the formation of impurity phases.

In order to overcome the limitations of static hydrothermal synthetic methods, we have adapted dynamic hydrothermal methods. Through these dynamic routes, $LiMn_2O_4$

*Corresponding authors. Tel.: +86 571 88320611; fax: +86 571 88320832.
*E-mail addresses:* jhyao@zjut.edu.cn (J. Yao), wanglb99@zjut.edu.cn (L. Wang).

0272-8842/$ - see front matter © 2012 Elsevier Ltd and Techna Group S.r.l. All rights reserved.
http://dx.doi.org/10.1016/j.ceramint.2012.07.093

was found to be of high purity, and the time to complete the synthesis reduced to 10 h. Furthermore, $LiMn_2O_4$ synthesized *via* dynamic hydrothermal routes had high lithium content and exhibited better electrochemical performance than the material obtained *via* static hydrothermal route.

## 2. Experimental

### 2.1. Synthesis

$LiMn_2O_4$ nanoparticles were synthesized using three types of hydrothermal methods, i.e.: 1) a normal static autoclave (sample obtained is denoted as *S*-LiMO), 2) a rotating Teflon-lined steel autoclave (*R*-LiMO), and 3) autoclave with stirring paddle in the reaction pot (*P*-LiMO), as schematically shown in Fig. 1. In the typical synthetic process, 0.486 g of lithium hydroxide monohydrate was dissolved in 15 mL of double-distilled water. 0.208 g of electrolytic manganese dioxide (EMD) and 0.363 mL of $Mn(NO_3)_2$ aqueous solution(50 wt%) were added while stirring at room temperature. The resulting mixtures were transferred into the respective autoclaves and heated at 150 °C for 10 h. After the hydrothermal treatment, the solid products were collected by vacuum filtration, washed several times with distilled water and then dried at 120 °C for 3 h.

### 2.2. Characterizations

The crystalline phases of the obtained materials were identified by powder X-ray diffraction (XRD, PANalytical, X'Pert Pro) with Cu Kα radiation ($\lambda = 0.154056$ nm) in the $2\theta$ range from 10° to 80° with a scan step of 0.03°. The morphology and structure of the materials obtained was determined by a scanning electronic microscopy (SEM, Hitachi S-4700, operated at 15.0 KV). In order to confirm the highly crystalline nature of the $LiMn_2O_4$ particles obtained by dynamic hydrothermal method, the *P*-LiMO material was examined by Transmission Electron Microscopy (TEM, FEI Tecnai G2-F30). The specific surface-area of the samples was measured by a BET (Brunauer–Emmett–Teller) surface-area analyzer (Micromeritics, ASAP2020).

The electrochemical performance of the as-prepared $LiMn_2O_4$ was evaluated by assembling a CR2032-type coin cell in an argon filled glove box. A CR2032-type coin cell consisted of the prepared $LiMn_2O_4$ samples as cathode, Li metal as the counter electrode and an electrolyte of 1 mol $L^{-1}$ $LiPF_6$ in a solvent mixture of ethylene carbonate (EC), dimethyl carbonate (DMC) and ethylmethyl carbonate (EMC) (1:1:1, v/v/v). The active material, acetylene black and polyvinylidene fluoride (PVDF) were grinded with a 1-methyl-2-pyrrolidinone (NMP) solution with the following weight ratio of 80:12:8 to form a slurry. This slurry was then casted onto an aluminum foil current collector and dried at 120 °C for 3 h.

Galvanostatic charge–discharge tests were performed over a voltage range of 3.3–4.3 V (vs. $Li/Li^+$) with a Land CT2001A battery test system at room temperature. Electrochemical impedance spectroscopy (EIS) was recorded with a Solartron Impedance/gain phase analyzer (model SI 1260) coupled to a potentiostat (SI 1287) over the frequency range from $10^{-2}$ Hz to $10^5$ Hz on the open circuit voltage at room temperature.

## 3. Results and discussion

XRD patterns of the as-prepared $LiMn_2O_4$ obtained by the three hydrothermal processes investigated are shown in Fig. 2. All peaks of the materials prepared *via* dynamic hydrothermal route show a pure single phase with a spinel structure in good agreement with that of $LiMn_2O_4$ (JCPDS No.35-0782) [13]. No other phases were detected by XRD. The sharp and intense peaks of *P*-LiMO and *R*-LiMO indicate highly crystalline. However, additional peaks corresponding to $Mn_3O_4$ and $Mn_2O_3$ were observed on the XRD pattern of *S*-LiMO prepared by the static route. This clearly indicates that under the same experimental conditions, the dynamic route is more effective for producing pure $LiMn_2O_4$. The XRD patterns for the three materials were also refined using Reflex module of Materials studio in order to determine any evolution of the lattice parameters. After refinement, lattice constants for *P*-LiMO, *R*-LiMO and *S*-LiMO were found to be of $8.235 \pm 3$ Å, $8.232 \pm 6$ Å and $8.221 \pm 1$ Å, respectively. A value somewhat

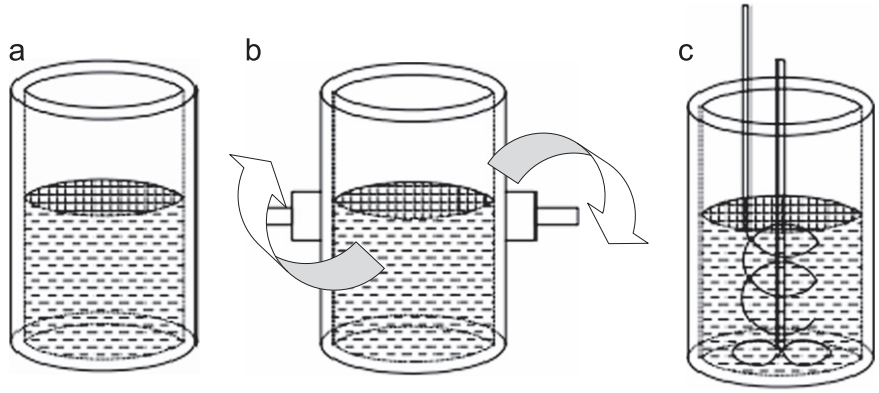


Fig. 1. Schematic illustration of three set-ups for hydrothermal synthesis: (a) static type; (b) rotating type and (c) using stirring paddle.

close to that reported in the literature for the $LiMn_2O_4$ spinel, i.e. 8.248 Å. Additional information on micro-structure was obtained by calculating the crystallite size of the materials using Debye–Scherrer equation $D = K\lambda/\beta \cos\theta$, and those were found to be of 391, 267, and $236 \pm 5$ nm for *S*-LiMO, *R*-LiMO, and *P*-LiMO, respectively (Table 1).

Morphologies of the material was further characterized by SEM (Fig. 3). Mainly small particles in the range of 200–300 nm were observed for *R*-LiMO and *P*-LiMO. However, for the static method larger particles with a size varying between 400 and 600 nm were also imaged by SEM. These larger particles are likely due to the agglomeration of reactants and/or products during the static hydrothermal synthesis.

To confirm the crystalline nature of the particles obtained by the dynamic method, TEM investigation was carried out on *P*-LiMO showing the lowest crystallite size (Fig. 4). TEM revealed that the *P*-LiMO particles have a rounded morphology with mean size of about 200 nm in agreement with SEM analysis (Fig. 3). Furthermore, the interplanar distance was found to be of 2.9145 Å, which corresponds to the (220) plane of $LiMn_2O_4$ phase (JCPDS No.35-0782). Therefore, TEM analysis confirmed the highly crystalline nature of the *P*-LiMO particles prepared *via* dynamic hydrothermal route in agreement with XRD results (Fig. 2).

Based on these results, the electrochemical properties of the materials were thus examined. Fig. 5 shows the initial EVS voltage profile and corresponding different capacity responses for *S*-LiMO, *P*-LiMO and *R*-LiMO electrode, respectively. From Fig. 5 it can be seen that that all three samples depict four redox peaks associated to the insertion and extraction of Li ions into the spinel structure. For example, *S*-LiMO displayed two oxidation peaks at ca. 3.97 and 4.14 V associated with the extraction of Li ions from the spinel structure and two reduction peaks at ca. 4.10 and 3.94 V that can be related to the insertion of Li within the spinel structure. The electrochemical properties of *S*-LiMO, *R*-LiMO and *P*-LiMO were further tested by

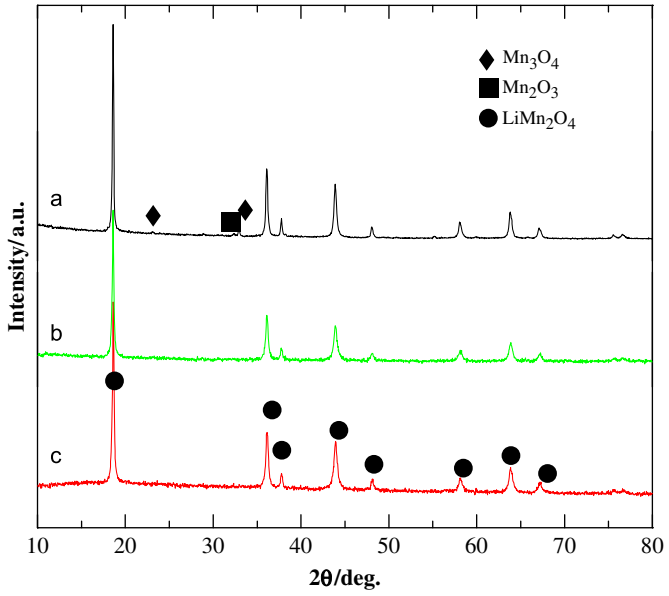


Fig. 2. XRD patterns for the as-synthesized and as-annealed samples: (a) *S*-LiMO; (b) *R*-LiMO; and (c) *P*-LiMO.

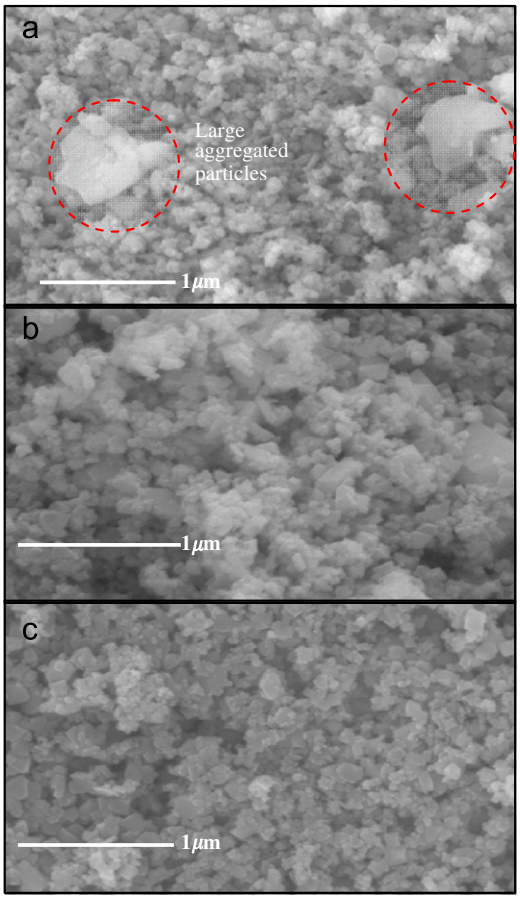


Fig. 3. SEM images for the as-synthesized samples: (a) *S*-LiMO; (b) *R*-LiMO; and (c) *P*-LiMO.

Table 1
Main characteristics of nanocrystalline $LiMn_2O_4$ powders synthesized by various hydrothermal routes.

| Samples | Condition of synthesis (150 °C, 10 h) | CSD size (XRD) ($\pm 5$ nm) | Mean particle size (SEM) (nm) | BET ($m^2/g$) | Phase composition |
|---|---|---|---|---|---|
| *S*-LiMO | Static | 392 | 360 | 72 | $LiMn_2O_4$, $Mn_2O_3$, $Mn_3O_4$ |
| *R*-LiMO | Rotating | 267 | 275 | 83 | $LiMn_2O_4$ |
| *P*-LiMO | Stirring | 236 | 240 | 88 | $LiMn_2O_4$ |

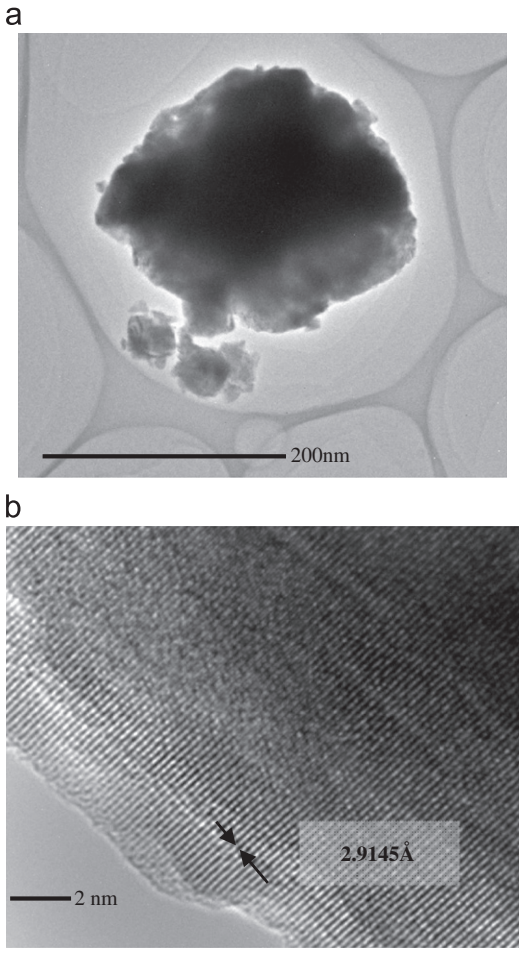


Fig. 4. TEM images of *P*-LiMO sample at (a) low and (b) high magnification.

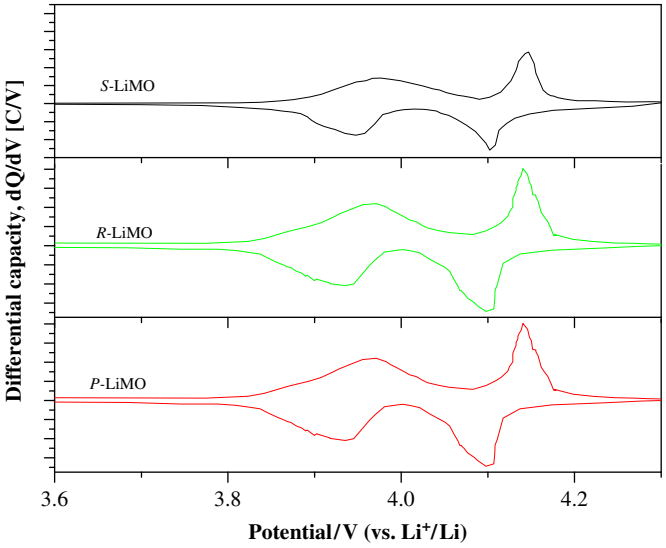


Fig. 5. EVS differential capacity data for *S*-LiMO, *R*-LiMO and *P*-LiMO electrodes.

galvanostatic charge–discharge cycling using CR2032-type coin cells at a current density of 0.5 C and between the cutoff voltages of 3.3 and 4.3 V. From Fig. 6(a), it can be

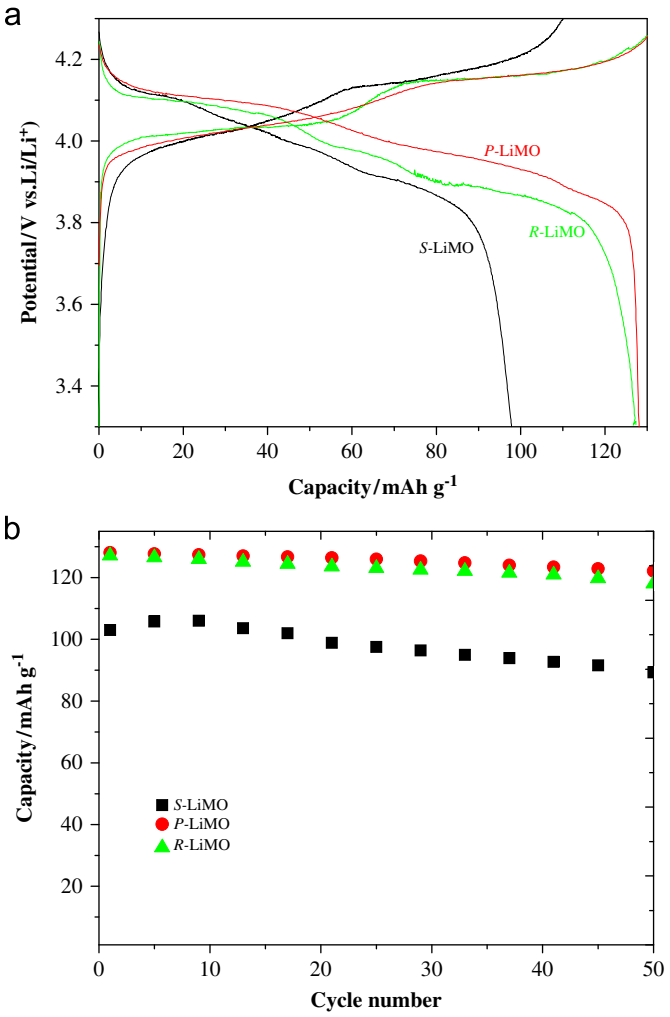


Fig. 6. Initial charge-discharge curves for the as-synthesized samples: (a) *S*-LiMO; (b) *R*-LiMO; and (c) *P*-LiMO. (b) Cycling properties of three samples.

seen that all the charge-discharge curves exhibit two potential plateaus at around 4.0 V, indicating a remarkable characteristic of spinel $LiMn_2O_4$ with a two-stage mechanism for $Li^+$ extraction and insertion [14]. The first plateau region of discharge curve would correspond to a two-phase equilibrium between $\lambda$-$MnO_2$ and $Li_xMn_2O_4$ ($0 < x < 0.5$), while the second plateau would be related to a phase equilibrium between $Li_xMn_2O_4$ ($0.5 < x < 1$) and $LiMn_2O_4$ [9–12]. It is noteworthy that the discharge plateau of *P*-LiMO is slightly higher than that of *R*-LiMO, and this may be due to faster lithiation kinetics for *P*-LiMO sample resulted from smaller particle sizes and higher spinel crystallinity [12–15]. Furthermore, the initial discharge capacity of *S*-LiMO was found to be of 97.9 mAh $g^{-1}$ only. By contrast, the materials obtained *via* the two dynamic hydrothermal processes displayed higher discharge capacity of 127.3 and 128.1 mAh $g^{-1}$ for *R*-LiMO and *P*-LiMO, respectively. Once again, such an improvement in performances would be related to the smaller particles/crystallite sizes resulting from the dynamic hydrothermal process. Furthermore, it is apparent that during

the dynamic synthesis a thorough reaction between $MnO_2$ and LiOH solution must be promoted and thus the effective intercalation of Li into the $MnO_2$ precursor leading to the formation of a Li-rich $LiMn_2O_4$.

In order to further evaluate the electrochemical performance of the three as-prepared materials, cycling tests were conducted. Fig. 6(b) illustrates that at a charge-discharge rate of 0.5 C, *P*-LiMO displayed excellent cycling behavior with a 95.3% capacity retention ability of 122.1 mAh $g^{-1}$ after 50 cycles. Similarly, *R*-LiMO displayed a capacity of 118 mAh $g^{-1}$ at the 50th cycle, i.e. a 92.6% capacity retention. In contrast, *S*-LiMO obtained by static hydrothermal method displayed a drastic fading in performances with only 83.5% of the capacity remained after 50 cycles. Such poor performances may results from a Li-deficient spinel structure as well as the formation of the impurities. That in turn would lead to a slow intercalation of Li [12–15].

To gain further understanding on the materials properties obtained by the two dynamic hydrothermal processes, Electrochemical Impedance Spectroscopy (EIS) measurement were carried out for *P*-LiMO and *R*-LiMO. Fig. 7 shows the Nyquist plots of the three as-prepared materials. The three materials displayed similar EIS patterns characterized by a typical semicircle in high-frequency range that would correspond to charge-transfer resistance and a straight line in the low-frequency range, which was attributed to the migration of Li-ions into the bulk of active mass. The equivalent circuits are shown in the inset on Fig. 7. By comparing the width of the semicircle from the impedance spectra, *P*-LiMO exhibited the smallest Rct which suggested that lithium-ion diffusion was easier in this material. This could be attributed to the ultrafine particle size and the good structural crystallinity of *P*-LiMO. Both would favor enhanced cycling performances.

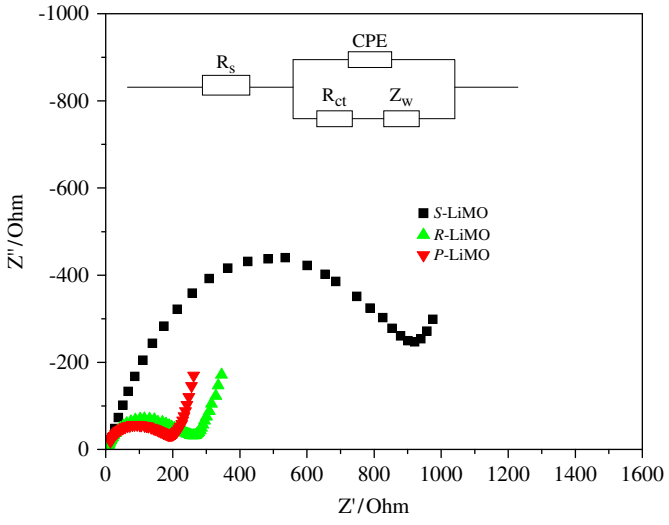


Fig. 7. Nyquist plots of *S*-LiMO, *R*-LiMO and *P*-LiMO samples, and the inserted is the equivalent circuit for the Nyquist plots of the *P*-LiMO sample. Rs is solution resistance, CPE is a constant phase associated with the charge-transfer resistance (Rct) and the Warburg impedance (Zw) which is due to the migration of Li-ions in the bulk materials.

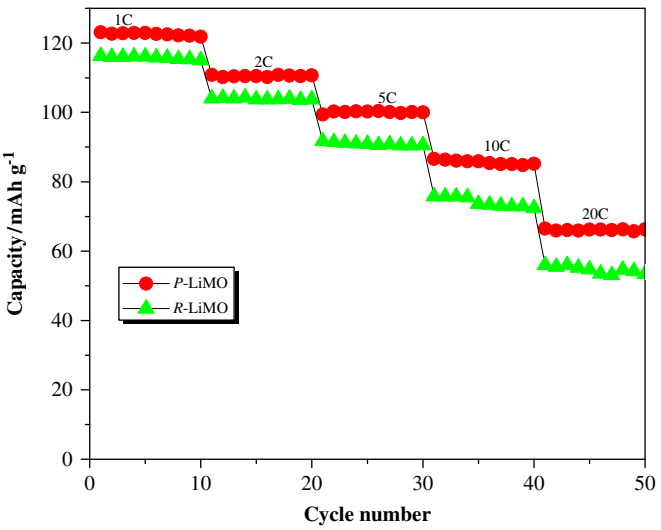


Fig. 8. Cycling performance of *R*-LiMO and *P*-LiMO samples at various rates.

The discharge capacity of *P*-LiMO and *R*-LiMO was also tested at different current densities (Fig. 8). Under this various current regimes, *P*-LiMO was found to perform the best as it reached a discharge capacity of 123.1, 113.6, 104.5, 92.2 and 73.9 mAh $g^{-1}$ at 1, 2, 5, 10 and 20C, respectively. This result is a significant improvement as compared to those reported in the literature for $LiMn_2O_4$ prepared *via* high-temperature solid-state reaction methods [15].

## 4. Conclusion

In summary, high purity $LiMn_2O_4$ with 200–300 nm in particle size can be obtained *via* dynamic hydrothermal synthesis within 10 h. The resulting material showed an initial discharge capacity of 128.3 mAh $g^{-1}$ and 95.3% capacity retention at 0.5 C. Meanwhile it showed a satisfactory high rate cycle performance and good high rate capability by delivering a capacity of 123.1 mAh $g^{-1}$ at 1 C, 113.6 mAh $g^{-1}$ at 2 C, 104.5 mAh $g^{-1}$ at 5 C, 92.2 mAh $g^{-1}$ at 10 C and 73.9 mAh $g^{-1}$ at 20 C. Therefore, dynamic hydrothermal synthesis may be a promising method for the large scale synthesis of $LiMn_2O_4$ with high electrochemical performance as cathode material.

## Acknowledgments

This work was supported by the International Science and Technology Cooperation Program of China (Grant no. 2012DFG42100), and the Doctoral Program of Higher Education of China (Grant no. 2011010113003), Zhejiang Provincial Natural Science Foundation of China (Grant no. LQ12B01003), Zhejiang University of Technology start-up fund (Grant no. 101009529), National Natural Science Foundation of China (NSFC, Grant no. 20506024) and the

State Key Development Program for Basic Research of china (Grant no. 2007CB216409).

## References

[1] T. Yuan, R. Cai, K. Wang, R. Ran, S. Liu, Z. Shao, Combustion synthesis of high-performance $Li_4Ti_5O_{12}$ for secondary Li-ion battery, Ceramics International 35 (5) (2009) 1757–1768.

[2] A. Kuwahara, S. Suzuki, M. Miyayama, High-rate properties of $LiFePO_4$/carbon composites as cathode materials for lithium-ion batteries, Ceramics International 34 (4) (2008) 863–866.

[3] M. Armand, J.M. Tarascon, Building better batteries, Nature 451 (7179) (2008) 652–657.

[4] X.L. Li, R.M. Xiang, T. Su, Y.T. Qian, Synthesis and electrochemical properties of nanostructured $LiMn_2O_4$ for lithium-ion batteries, Materials Letters 61 (17) (2007) 3597–3600.

[5] J.H. Yao, X.T. Wu, P.J. Zhang, S.S. Wei, L.B. Wang, Effects of $Li_2CO_3$ as a secondary lithium source on the $LiFePO_4$/C composites prepared via solid-state method, Journal of Physics and Chemistry of Solids 73 (2012) 803–807.

[6] Y.Y. Xia, T. Sakai, T. Fujieda, X.Q. Yang, X. Sun, Z.F. Ma, J. McBreen, M. Yoshio, Correlating capacity fading and structural changes in $Li_{1+y}Mn_{2-y}O_{4\text{-delta}}$ spinel cathode materials—a systematic study on the effects of Li/Mn ratio and oxygen deficiency, Journal of the Electrochemical Society 148 (7) (2001) A723–A729.

[7] J.H. Yao, C.q. Shen, P.J. Zhang, D.H. Gregory, L.B. Wang, Enhanced cycle ability of spinel $LiMn_2O_4$ by controlling the phase purity and structural strain, Journal of Physics and Chemistry of Solids, 73 (2012) doi 10.1016/j.jpcs.2012.07.006.

[8] J.Y. Luo, Y.G. Wang, H.M. Xiong, Y.Y. Xia, Ordered mesoporous spinel $LiMn_{(2)}O_{(4)}$by a soft-chemical process as a cathode material for lithium-ion batteries, Chemistry of Materials 19 (19) (2007) 4791–4795.

[9] Y. Wang, G.Z. Cao, Developments in nanostructured cathode materials for high-performance lithium-ion batteries, Advanced Materials 20 (12) (2008) 2251–2269.

[10] T.-F. Yi, Y.-R. Zhu, X.-D. Zhu, J. Shu, C.-B. Yue, A.-N. Zhou, A review of recent developments in the surface modification of $LiMn_2O_4$ as cathode material of power lithium-ion battery, Ionics 15 (2009) 779–784.

[11] H. Yue, X. Huang, D. Lv, Y. Yang, Hydrothermal synthesis of $LiMn_2O_4$/C composite as a cathode for rechargeable lithium-ion battery with excellent rate capability, Electrochimica Acta 54 (23) (2009) 5363–5367.

[12] K. Kanamura, K. Dokko, T. Kaizawa, Synthesis of spinel $LiMn_2O_4$ by a hydrothermal process in supercritical water with heat-treatment, Journal of the Electrochemical Society 152 (2) (2005) A391–A395.

[13] W. Tang, X.J. Wang, Y.Y. Hou, L.L. Li, H. Sun, Y.S. Zhu, Y. Bai, Y.P. Wu, K. Zhu, T. van Ree, Nano $LiMn_2O_4$ as cathode material of high rate capability for lithium ion batteries, Journal of Power Sources 198 (2012) 308–311.

[14] C.H. Lu, S.W. Lin, Influence of the particle size on the electrochemical properties of lithium manganese oxide, Journal of Power Sources 97–8 (2001) 458–460.

[15] T. Kakuda, K. Uematsu, K. Toda, M. Sato, Electrochemical performance of Al-doped $LiMn_2O_4$ prepared by different methods in solid-state reaction, Journal of Power Sources 167 (2) (2007) 499–503.